

Revised Orbital, Physical, Stability, and Habitability Parameters of the Binary System HD 25811 Using Gaia Observations

Hassan B. Haboubi¹, Mashhoor A. Al-Wardat^{1,2}, Ahmad A. Abushattal³, Maximiliano Dirk⁴, Hatem Widyan⁵, Naufa Nazar¹, Joshua V. Thomji⁶, and Suhail Masda⁷

Department of Applied Physics and Astronomy, College of Sciences, University of Sharjah, P.O. Box 27272 Sharjah, United Arab Emirates
 Sharjah Academy for Astronomy, Space Sciences and Technology, University of Sharjah, P.O. Box 27272 Sharjah, United Arab Emirates
 Department of Physics, Al-Hussein Bin Talal University, P.O. Box 20, Ma'an, 71111, Jordan

⁴ Centre for Astrophysics Research, University of Hertfordshire, Hatfield, AL10 9AB, UK
⁵ Department of Physics, Al al-Bayt University, P.O. Box 20, Mafraq, 25113, Jordan

Received 2025 May 28; revised 2025 September 5; accepted 2025 September 12; published 2025 October 23

Abstract

Al-Wardat's method is used in this research to analyze the two components of the HD 25811 binary system, which combines the results of speckle interferometry with the astrometric data to construct the synthetic spectral energy distribution of the system. The method results in the effective temperatures at $7100 \pm 50 \, \text{K}$ for component A and $7000 \pm 50 \, \text{K}$ for component B, while their masses measure as $1.65 \pm 0.15 \, M_{\odot}$ for component A and $1.58 \pm 0.14 \, M_{\odot}$ for component B. The system exists at an estimated age of $0.794 \, \text{Gyr}$, while both stars remain in their initial subgiant evolutionary phase. The evolutionary tracks together with isochrones for Z = 0.03 validate that the system components share both their origin and chemical compositions. The orbital analysis shows that the system has a period of $15.97 \, \text{yr}$ and an eccentricity of 0.713, while the total system mass amounts to $3.65 \pm 0.49 \, M_{\odot}$. We detailedly analyze the system's orbital dynamics to assess planetary stability and habitability zones, which lead to the dynamics of circumbinary (P-type) and circumstellar (S-type) orbits using empirical criteria, revealing large regions in which planetary orbits remain dynamically stable. Luminosities and effective temperatures of each stellar component are used to determine their habitable zones.

Key words: (stars:) binaries (including multiple): close – (stars:) binaries: visual – (stars:) binaries: spectroscopic – stars: evolution – Astrometry and Celestial Mechanics

1. Introduction

The investigation of binary stars provides essential insights into stellar physical processes. These systems allow us to make accurate measurements of fundamental stellar properties, including stellar mass, radius and luminosity to validate stellar evolutionary models and star formation theories (Andersen 1991; Al-Wardat et al. 2017; Docobo et al. 2017). The observation of close or unresolved binary stars through conventional telescopes becomes extremely difficult because researchers cannot observe the individual stars of the binary and multiple systems. As a result, astronomers need to use indirect methods to separate overlapping light signals enabling them to determine orbital dynamics, temperature ratios, and evolutionary stages by using innovative computational and observational techniques (Abushattal et al. 2019a, 2019b; Algnamat et al. 2022; Hussein et al. 2022). Al-Wardat's method for analyzing stellar systems is instrumental in utilizing synthetic spectral energy distribution (SED) to handle these complex situations (Al-Wardat 2012; Al-Wardat et al. 2014a, 2016, 2021a). Al-Wardat's method combines observed photometric data with theoretical stellar atmosphere models to reconstruct the separate contributions of binary system stars which remain unresolved spatially. This method provides accurate measurements of stellar physical parameters such as effective temperatures ($T_{\rm eff.}$), surface gravities (Log g), and metallicity (Z) (Al-Wardat et al. 2021a; Masda & Al-Wardat 2023; Masda et al. 2023, 2025) by reducing the uncertainties based on the traditional method. The method serves as a standard tool for analyzing visual and spectroscopic binaries, and has improved research on stellar populations, exoplanet host stars and distance measurements (see: Al-Wardat 2014; Masda et al. 2016, 2018; Al-Wardat et al. 2021b; Masda et al. 2021; Masda et al. 2023).

Most nearby stars are members of binary or multiple systems, which are important in modern astrophysical research. These systems allow for the observation of stellar formation, evolution, and dynamics. In the last few decades, astronomical measurements have been made possible with unprecedented precision via astrometric and spectroscopic advances, thanks to missions such as Hipparcos (ESA 1997)

⁶ Division of Artificial Intelligence and Machine Learning, Karunya Institute of Technology and Sciences, Coimbatore, Tamil Nadu, 641114, India

⁷ Department of Physics, Mahrah University, Mahrah, Yemen

and Gaia (Gaia Collaboration et al. 2016). By combining astrometric and photometric data of binary systems, astronomers can derive stellar masses, orbital parallaxes, and three-dimensional orbital solutions. It is essential to know these fundamental stellar parameters to understand stellar physics and also to understand the environment in which exoplanets form (Docobo et al. 2018; Abushattal et al. 2022a, 2022b; Alameryeen et al. 2022).

Cannon & Pickering (1933) classified the spectral types of the HD 25811 binary star system as F8V for the primary component and G9V for the secondary component. In 2014, Al-Wardat et al. (2014b) analyzed the system and they classified the system as a subgiant system. Al-Wardat et al. (2014b) estimated the stellar parameters of the system such as the effective temperatures at $6850 \pm 50 \,\mathrm{K}$ for component A and $7000 \pm 50 \, \text{K}$ for component B. At the time, there were no direct measurements of trigonometric parallax. In spite of this, the study found that the components have masses of $M_a = 1.55 \pm 0.16 \, M_{\odot}$ and $M_b = 1.50 \pm 0.15 \, M_{\odot}$, and a dynamical parallax of $\pi = 5.095 \pm 0.095$ mas (corresponding to a distance of $d = 196.2 \,\mathrm{pc}$). The initial value of $\pi = 5.24 \pm 0.6$ mas (or d = 191 pc), as reported by Al-Wardat (2003), was used for this estimation. Since then, important progress has been made, mainly with the release of Gaia astrometric data which now allow for accurate parallaxes and observations in photometry across several data releases (Gaia DR1-DR3). Because of Gaia's high-quality astrometric data and new speckle interferometry, we have decided to revisit the stellar and orbital parameters of HD 25811. Using Gaia data, this study enhances the accuracy of previous parameter results and provides a better understanding of the system's evolution, stability and habitability zones.

We will apply Al-Wardat's method for analyzing binary and multiple systems, a combination of photometric observations and synthetic SEDs, to determine the fundamental stellar parameters of both components based on new results of speckle interferometry and observational SED of Gaia. This method is a novel and viable method to study binary systems in which it is difficult to resolve individual components directly (Al-Wardat 2002a, 2003, 2007, 2009). We will show how this technique can be applied to study the properties of the binary star HD 25811. HD 25811 is a binary star system in the constellation Taurus, about 202.55 pc (Gaia Collaboration 2020) from our planet. The system contains two B-type mainsequence stars and its primary is classified as F0 E (Cannon & Pickering 1933). This system has an apparent magnitude of 8.67 (Høg et al. 2000) and its two stars differ in magnitude by about 0.2.

Binary system stability is crucial when assessing planetary formation and orbital survival potential. By measuring stellar mass, semimajor axis, luminosity, and orbital inclination, researchers can estimate orbital stability zones around each component or within circumbinary configurations. The zone of

Table 1
Observational Data of the HD 25811 System

Parameter	Value	Reference
R.A. (J2000)	04h06m16s41	Gaia Collaboration (2022)
decl. (J2000)	+19°52′28″56	Gaia Collaboration (2022)
$\Delta m \text{ (mag)}$	0.20	INT4
$\pi_{\mathrm{DR}1}$ (mas)	5.22	Gaia Collaboration et al.
		(2016)
π_{DR2} (mas)	4.953 ± 0.081	Gaia Collaboration (2018)
$\pi_{DR3}(mas)$	4.937 ± 0.072	Gaia Collaboration (2020)
E(B-V) (mag)	0.748	Schlafly & Finkbeiner (2011)
A_{v} (mag)	0.239	Schlafly & Finkbeiner (2011)
Spectral type	F0	ESA (1997)
	Photometric	
	Observations	
V _J (mag)	8.67 ± 0.02	ESA (1997)
$(B - V)_{\rm J}$ (mag)	0.389 ± 0.028	ESA (1997)
Tycho-2 B mag, $B_{\rm T}$	9.11	Høg et al. (2000)
Tycho-2 V mag, $V_{\rm T}$	8.71	Høg et al. (2000)
2MASS J mag, J	7.857 ± 0.02	Cutri et al. (2003)
2MASS H mag, H	7.764 ± 0.02	Cutri et al. (2003)
Gaia B_P mag, B_P	8.759	Gaia Collaboration (2022)
Gaia $R_{\rm P}$ mag, $R_{\rm P}$	8.243	Gaia Collaboration (2022)

stability is crucial in determining where a planet might retain a stable orbit over astronomical timescales, especially when the planet's gravity perturbs both stars. By identifying dynamically stable regions where life might exist in systems containing these conditions, the foundation is laid for identifying possible life-sustaining planets (Abushattal et al. 2024). The habitability of a binary system depends not only on its orbital stability but also on its radiative environment. For each star, luminosity and temperature parameters can be used to calculate the habitable zone (HZ), where liquid water might exist on its surface. As part of this study, we model these HZs in binary systems, combining spectroscopic and visual solutions to enhance accuracy. A key research objective is to identify binary systems with stable planet orbits and favorable conditions for life, which will advance the ongoing search for Earth-like exoplanets in complex stellar environments.

2. Observational Data

Observational data of the system such as photometric data and SED are taken from different sources, which are used in the study of the HD 28511 system to examine its stellar components. The photometric observations are taken from Tycho-2 (Høg et al. 2000), 2MASS (Cutri et al. 2003), and Gaia (Gaia Collaboration 2022), while the observational SED of the HD 25811 system was taken from Al-Wardat (2002b). The observational data of the system are given in Table 1

Table 2
Astrometric Measurements for HD 25811 Used to Estimate Orbital Parameters with Our MCMC Code

Epoch of			
Observation	θ	$\rho \pm \sigma$	Reference
	(deg)	(arcsec)	
1984.1127	66.7	0.0701 ± 0.01	Schmidtke & Africano (1984)
1984.1127	74.4	0.0653 ± 0.01	Evans et al. (1985)
1984.1127	74.4	0.0663 ± 0.01	Evans et al. (1985)
1984.846	81.0	0.066 ± 0.05	Balega & Balega (1987)
1985.8406	65.4	0.075 ± 0.05	McAlister et al. (1987)
1986.6573	64.8	0.072 ± 0.05	Balega et al. (1989)
1986.8862	59.9	0.074 ± 0.05	McAlister et al. (1989)
1986.889	60.6	0.079 ± 0.05	McAlister et al. (1989)
1987.7655	56.9	0.074 ± 0.05	McAlister et al. (1989)
1988.6609	52.2	0.073 ± 0.05	McAlister et al. (1990)
1989.7067	41.5	0.076 ± 0.05	Hartkopf et al. (1992)
1989.8077	37.7	0.068 ± 0.05	Balega et al. (1994)
1990.7551	21.9	0.078 ± 0.05	Hartkopf et al. (1992)
1993.8419	353.0	0.056 ± 0.05	Balega et al. (1994)
1997.808	96.9	0.0582 ± 0.04	Balega et al. (2001)
1998.7747	86.9	0.06 ± 0.02	Balega et al. (2002)
1999.8185	79.4	0.0681 ± 0.01	Balega et al. (2004)
1999.8213	78.9	0.0683 ± 0.01	Balega et al. (2004)
2001.7614	67.3	0.076 ± 0.02	Balega et al. (2006)
2001.7614	66.9	0.076 ± 0.01	Balega et al. (2006)
2002.797	60.78	0.088 ± 0.005	Al-Wardat et al. (2014b)
2004.8158	49.0	0.074 ± 0.02	Balega et al. (2007)
2015.9105	78.3	0.0709 ± 0.005	Tokovinin et al. (2016)
2017.9319	63.6	0.0771 ± 0.003	Tokovinin et al. (2019)
2017.9319	65.6	0.0769 ± 0.005	Tokovinin et al. (2019)
2018.8409	61.1	0.0769 ± 0.005	Tokovinin et al. (2019)
2019.8569	55.6	0.0769 ± 0.005	Tokovinin et al. (2020)
2020.9272	49.0	0.0742 ± 0.001	Tokovinin et al. (2021)
2021.7981	41.9	0.0701 ± 0.002	Tokovinin et al. (2022)
2022.6857	36.9	0.0541 ± 0.005	Mason et al. (2023)
2023.9105	26.1	0.0551 ± 0.005	Tokovinin et al. (2024)

including photometric data, spectral types, and magnitude differences, as well as parallaxes, which are provided by different sources.

In Table 2 we report the astrometric measurements from the Fourth Catalog of Interferometric Measurements of Binary Stars (INT4), along with new speckle observations obtained with the HRCam@SOAR telescope. The first column lists the epoch of observation, the second lists the position angle of the secondary relative to the primary star (measured from north), the third lists the angular separation between the stars, while the fourth lists the reference for each entry.

3. Al-Wardat's Method

The analysis begins with the use of the new magnitude difference between the components of the system as $\Delta m = 0.20$ instead of $\Delta m = 0.23$ by Al-Wardat et al. (2014b). The difference between the two values will be appear

in radii of the individual components of the system, while the system's visual magnitude is estimated as $m_v = 8 \cdot 67 \pm 0.02$. The flux ratio is calculated as:

$$\frac{f_1}{f_2} = 2.512^{-\Delta m},\tag{1}$$

$$m_{\nu} = -2.5 \log(f_1 + f_2).$$
 (2)

The combination of these equations can lead to the estimate of the apparent magnitudes of both components as follows:

$$m_v^{(A)} = m_v + 2.5 \log(1 + 10^{-0.4 \, \Delta m}),$$
 (3)

$$m_{v}^{(B)} = m_{v}^{(A)} + \Delta m.$$
 (4)

The errors in the magnitudes are given by:

$$\sigma_{m_{\nu}^{(A)}}^{2} = \sigma_{m_{\nu}}^{2} + \left(\frac{1}{1 + 10^{+0.4 \,\Delta m}}\right)^{2} \sigma_{\Delta m}^{2},\tag{5}$$

$$\sigma_{m.(B)}^2 = \sigma_{m.(A)}^2 + \sigma_{\Delta m}^2.$$
 (6)

Next, we calculate the absolute magnitude M_{ν} for each component using the apparent magnitudes, distance d (in parsecs), and extinction A_{ν} of the system as follows

$$M_{v} = m_{v} + 5 - 5\log(d) - A_{v}. \tag{7}$$

The errors in the absolute visual magnitude for both components are given by:

$$\sigma_{M^{(A)}}^2 = \sigma_{m^{(A)}}^2 + (\ln(0.2\pi))^2 \sigma_{\pi}^2, \tag{8}$$

$$\sigma_{M^{(B)}}^2 = \sigma_{m^{(B)}}^2 + (\ln(0.2\pi))^2 \sigma_{\pi}^2. \tag{9}$$

Using the absolute magnitudes, we estimate the effective temperature and bolometric correction from Lang (1992) and Gray (2021). The bolometric magnitude is then determined by

$$M_{\text{bol}} = M_{\nu} + \text{BC}. \tag{10}$$

With the bolometric magnitude, the luminosity of each component is given by

$$M_{\text{bol}} - M_{\odot,\text{bol}} = -2.5 \log \left(\frac{L}{L_{\odot}}\right).$$
 (11)

Using the luminosity, the radii of the components are calculated as

$$\log\left(\frac{R}{R_{\odot}}\right) = 0.5\log\left(\frac{L}{L_{\odot}}\right) - 2\log\left(\frac{T}{T_{\odot}}\right). \tag{12}$$

The mass of each component is estimated using its radius or spectral type, referencing tables from Lang (1992). Finally, the surface gravity is determined as

$$\log(g) = \log\left(\frac{M}{M_{\odot}}\right) - 2\log\left(\frac{R}{R_{\odot}}\right) + 4.43. \tag{13}$$

The synthetic photometry technique is employed to validate the accuracy of the synthetic SEDs and to compare with the

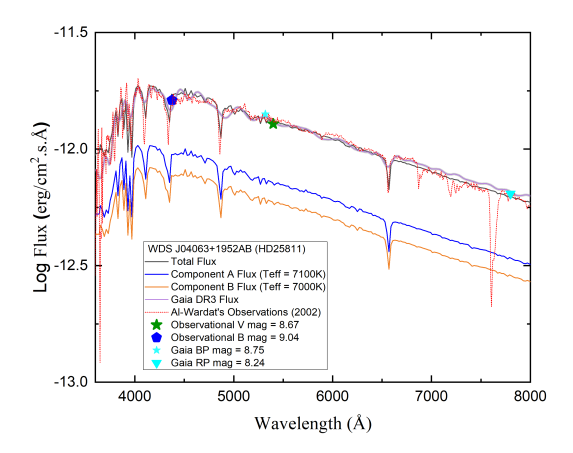


Figure 1. SED of HD 25811, showing the combined synthetic SED of the binary system along with individual flux contributions from each component. The observed fluxes were taken from Gaia DR3 (Gaia Collaboration 2020) and from Al-Wardat (2002b).

photometric observations of the system. To compute the synthetic magnitudes, we utilize a program based on the equation

$$m_p = -2.5 \log \frac{\int P_p(\lambda) F_{\lambda,s}(\lambda) d\lambda}{\int P_p(\lambda) F_{\lambda,r}(\lambda) d\lambda} + ZP_p, \tag{14}$$

where:

- m_p : synthetic magnitude for the passband p,
- $P_p(\lambda)$: dimensionless sensitivity function of the passband p,
- $F_{\lambda,s}(\lambda)$: synthetic SED of the object,
- $F_{\lambda,r}(\lambda)$: SED of the reference star Vega,
- ZP_p: zero-point calibration of the reference star Vega (Sterken 2007).

The best fit between the synthetic and observed photometry of the system will lead to the best fundamental stellar parameters and the dynamical results of the binary system.

4. Results and Discussions

4.1. Spectral Energy Distributions

The iteration process of Al-Wardat's method resulted in building the SEDs of the subcomponents in addition to the entire one of HD 25811, which in turn was compared with photometric and spectrophotometric observations.

The best fits between these synthetic SEDs and observed magnitudes, SEDs of Al-Wardat (2002b) and Gaia DR3, are shown in Figures 1 and 2.

The figures show clearly that the total flux (black line) agrees well with the combined fluxes of the component A ($T_{\rm eff}=7100~{\rm K}$) and component B ($T_{\rm eff}=7000~{\rm K}$), confirming

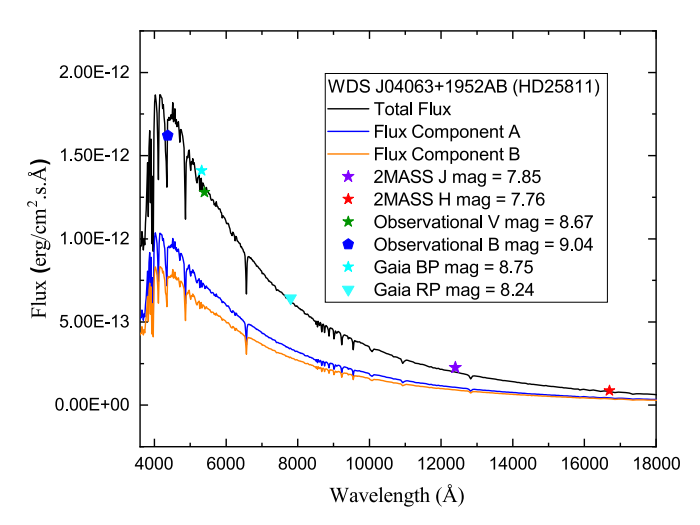


Figure 2. SED of HD 25811, showing the combined synthetic SED of the binary system along with individual flux contributions from each component. The observational magnitudes from Gaia (Gaia Collaboration 2020), Tycho-2 (Høg et al. 2000) and 2MASS (Cutri et al. 2003) are plotted for comparison.

Filter	Synthetic Total	Observed Total	Synthetic Star A	Synthetic Star B
B Johnson	9.07	9.04 ± 0.02	9.71	9.94
V Johnson	8.67	8.67 ± 0.02	9.33	9.54
R Cousins	8.17		8.83	9.02
I Cousins	7.88		8.54	8.73
J 2MASS	8.02	7.85 ± 0.02	8.69	8.86
H 2MASS	7.79	7.76 ± 0.02	8.47	8.63
G Gaia	8.64	8.58 ± 0.002	9.30	9.50
Bp Gaia	8.80	8.75 ± 0.002	9.45	9.66
Rp Gaia	8.32	8.24 ± 0.002	8.99	9.17
B-V	0.393	0.370 ± 0.03	0.386	0.40
Bp - Rp	0.474	0.515	0.461	0.490

their nearly identical effective temperatures. Compared with Al-Wardat et al. (2014b), the results of our analysis are the best based on newly observed SEDs from Gaia and new measurements from speckle interferometry. In addition, the observational magnitudes of the system (V = 8.67, B = 9.04) are consistent with the synthetic magnitudes of the revised stellar parameters of the system.

Based on the synthetic SEDs and Equation (14), we calculated the synthetic magnitudes and color indices of the total system and the components as listed in Table 3. We can see that the best fit between the combined synthetic and observed photometry of the system is achieved. This strong correlation can be considered as a kind of confirmation of the reliability of our approach and the stellar parameters of the

 $\begin{tabular}{ll} \textbf{Table 4} \\ \textbf{The Revised Stellar Parameters for Components A and B of HD 25811} \\ \end{tabular}$

Parameter	Unit	Component A	Component B
$M_{\nu} \pm \sigma_{M_{\nu}}$	(mag)	2.77 ± 0.02	3.00 ± 0.03
$M_{ m bol}\pm\sigma_{M_{ m bol}}$	(mag)	2.57 ± 0.01	2.73 ± 0.02
$L \pm \sigma_L$	(L_{\odot})	7.39 ± 0.19	6.37 ± 0.14
$T_{ m eff}\pm\sigma_{T_{ m eff}}$	(K)	7100 ± 50	7000 ± 50
$R \pm \sigma_R$	(R_{\odot})	1.88 ± 0.20	1.76 ± 0.01
$M \pm \sigma_M$	(M_{\odot})	1.65 ± 0.13	1.58 ± 0.11
$\log(g) \pm \sigma_{\log(g)}$	(cm s^{-2})	4.14 ± 0.01	4.17 ± 0.02
Spectral Type	(-)	F0	F1

system. This correspondence further supports the validity of the method and confirms the credibility of the determined stellar parameters as listed in Table 4. Compared with Al-Wardat et al. (2014b), the radii of the individual components of the system are estimated as $1.88 \pm 0.20 \, R_{\odot}$ and $1.76 \pm 0.01 \, R_{\odot}$ for the primary and secondary component, respectively, instead of $1.96 \pm 0.20 \, R_{\odot}$ and $1.69 \pm 0.20 \, R_{\odot}$ by Al-Wardat et al. (2014b).

The synthetic evolutionary tracks of the HD 25811 binary system, computed for a metallicity of Z=0.03, are presented in Figure 3. The tracks depict the components' evolution in the $\log T_{\rm eff}$ -luminosity plane, with components A and B. Based on metallicity and isochrone tracks, the system's age is estimated at $0.794~\rm Gyr$, with component A exhibiting a higher mass of $1.65M~\odot$ compared to component B of $1.58M~\odot$ as inferred from their positions along the tracks. Both stars lie near the main sequence, suggesting early evolutionary stages, with component A slightly more evolved.

The results obtained from both synthetic evolutionary tracks and SED fitting methods converge on a self-consistent model for the system, reinforcing the classification of HD 25811 as a binary system in the beginning of the subgiant phase. Although our findings leave the components just above the main sequence and in line with an early subgiant evolutionary stage, they do not exclude, in principle, an alternative pre-main-sequence (pre-MS) status to account for their location in the HR diagram. Nevertheless, the inferred ages (0.79 Gyr), metallicity (Z = 0.03) and the consistency between our spectroscopic/photometric properties and post-MS evolutionary tracks support the subgiant scenario. The existence of a pre-MS phase of stars of 1.6 M_{\odot} would suggest an age of just a few tens of Myr, which is not in agreement with the kinematics, metallicity and absence of star-forming regions in the system. The stellar mass and age estimations from the HR diagram align well with those inferred.

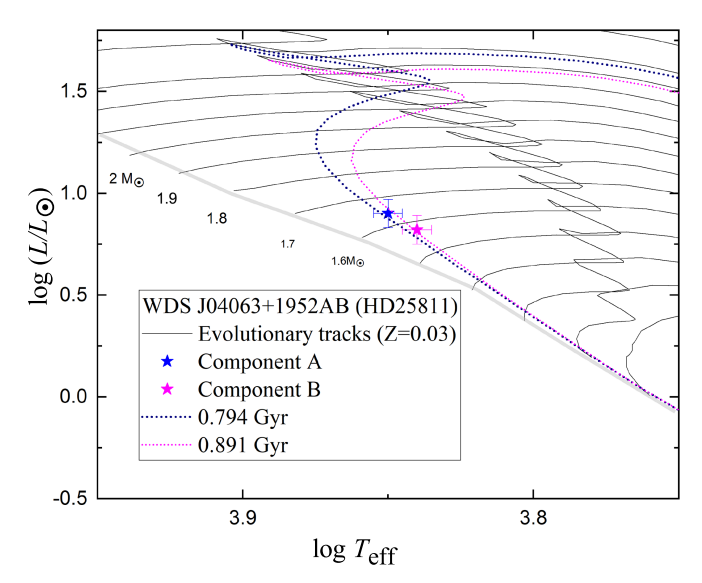


Figure 3. Components A and B of HD 25811 on the synthetic evolutionary and isochrone tracks of Z = 0.03 taken from Girardi et al. (2000a, 2000b).

4.2. Orbital Solution

Using the observations in Table 2, we calculated the orbital elements of the orbit using a Bayesian Markov Chain Monte Carlo (MCMC) code, as described in detail in Mendez et al. (2017) and Claveria et al. (2019). We ran our code using the previous solution of the orbits as prior information. One advantage of this approach is to generate posterior probability density functions (PDFs) for each orbital element, as well as the total mass of the system assuming a given parallax.

We present the best orbital parameters of the system, based on MCMC code, in Table 5. In this table, the first row indicates the maximum a posteriori (MAP) value, while the second row indicates the median of the a posteriori distribution, along with the intervals of the first (Q25) and third (Q75) quartiles as lower and upper values, respectively. Rows 3–5 show the old orbital solutions from Al-Wardat (2002b, 2014) and Balega et al. (2001). The orbital parameters were estimated using the Gaia DR3 parallax of 4.93 ± 0.0721 mas.

Figure 4 shows the orbit using the MAP values, the dashed red line indicates the line of nodes, while the dashed black and green lines indicate the position of periastron and apastron respectively. The smaller and darker points indicate the measurements with less uncertainty; the opposite is true.

Figure 5 shows the marginal posterior distribution of the orbital parameters. The vertical red lines indicate the MAP values, while the horizontal black bars indicate the range of the quartiles Q25–Q75. Figure 6 shows the pair marginal posterior distributions of the parameters.

The marginal distributions indicate that the period of this system is well-constrained. The observations cover just around half of the orbit and data with higher precision cover

	P (yr)	T (yr)	e	a (arcsec)	ω (deg)	Ω (deg)	i (deg)	$m_{ m tot} \ (M_{\odot})$
This Work (MAP)	15.94	1995.67	0.651	0.0492	205	75	139	3.89
This Work (Median)	$15.87^{+0.17}_{-0.17}$	$1995.1^{+0.38}_{-0.36}$	$0.733^{+0.025}_{-0.033}$	$0.0467^{+0.0027}_{-0.0014}$	206^{+36}_{-38}	78^{+37}_{-28}	155^{+12}_{-13}	$3.37^{+0.59}_{-0.28}$
Al-Wardat (2002a) Al-Wardat (2002b)	$31.00^{+1.33}_{-1.33}$	1981^{+12}_{-12}	$0.007^{+0.032}_{-0.032}$	$0.076^{+0.001}_{-0.001}$	291^{+140}_{-140}	61^{+1}_{-1}	124^{+2}_{-2}	$3.81^{+0.45}_{-0.45}$
Balega et al. (2001)	30.68	1990.96	0.045	0.079	32	50	128	4.37
Al-Wardat et al. (2014a) Al-Wardat et al. (2014b)	$32.99^{+2.37}_{-2.37}$	$1993.26^{+18.76}_{-18.76}$	$0.047^{+0.040}_{-0.040}$	$0.076^{+0.002}_{-0.002}$	68^{+216}_{-216}	59^{+3}_{-3}	123^{+3}_{-3}	$3.36^{+0.60}_{-0.60}$

Table 5
Estimated Orbital Elements Comparison, Including MCMC Results for HD 25811

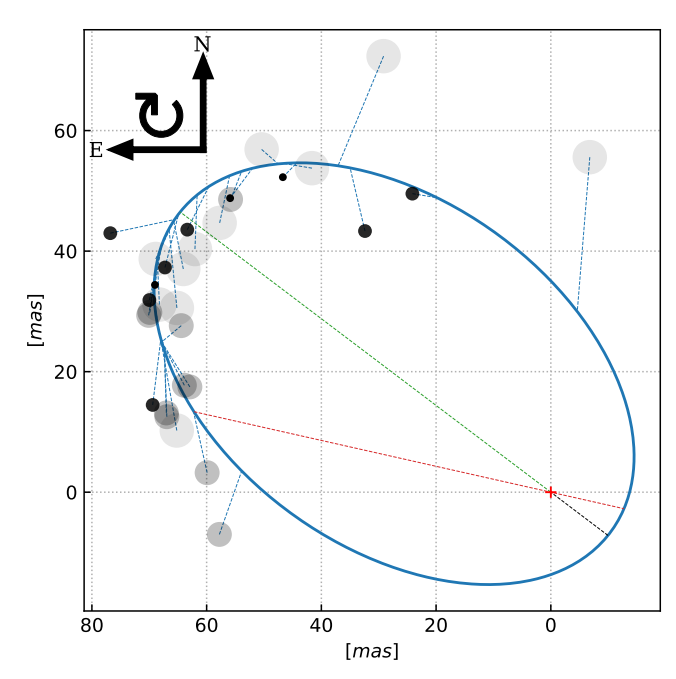


Figure 4. Orbit of HD 25811 using the MAP parameters.

approximately a third of the orbit. This could explain the major uncertainties in the angular parameters. The uncertainty in the angular parameters causes the semimajor axis to have an extended tail in the distribution, affecting the estimation of the total mass of this system. The fact that several observations are made in the pre-and post-apoastron passage helps to set a good constraint on the time of the periastron passage (*T*).

Observing the empty zone of this system with good precision will help in the constraint of the angular parameters. Radial velocity observations are also recommended for this purpose. The last observation is for the end of 2023, and considering that the period of this system is $\sim\!16\,\mathrm{yr}$, there is time to make a good observing plan.

5. Stability and Habitability of HD 25811

5.1. Stability Analysis

Orbital stability is inherently complex due to numerous influencing factors, including initial conditions, mathematical

frameworks, and physical constants (Szebehely 1984). In the context of binary star systems, an orbit is typically considered stable if the primary orbital parameters, eccentricity, semimajor axis, and inclination, remain relatively unchanged over extensive periods.

Habitability, as defined by Cockell et al. (2016), refers to the ability of an environment to support the metabolic processes of at least one known organism, thus allowing its survival, growth, and reproduction.

This study employs the empirical stability equations derived by Holman & Wiegert (1999) to delineate the stable orbital zones around the HD 25811 binary system. Two orbital types are examined: circumstellar (S-type), where a planet orbits a single star, and circumbinary (P-type), where a planet orbits both stars. Critical stability boundaries for these scenarios depend primarily on the binary's semimajor axis, mass ratio, and eccentricity.

To assess orbital stability within the HD 25811 system, we apply the empirical expressions of Holman & Wiegert (1999) for S-type and P-type orbits. The critical semimajor axis for S-type orbits is given by:

$$a_s = a [(0.464 \pm 0.006) + (-0.380 \pm 0.010) \mu + (-0.631 \pm 0.034) e + (0.586 \pm 0.061) \mu e + (0.150 \pm 0.041) e^{2} + (-0.198 \pm 0.047) \mu e^{2}]$$

For P-type orbits, the critical semimajor axis is:

$$\begin{split} a_p &= a \; [(1.60 \pm 0.04) + (4.12 \pm 0.09) \; \mu \\ &+ (5.10 \pm 0.05) \; e + (-4.27 \pm 0.17) \; \mu e \\ &+ (-2.22 \pm 0.11) \; e^2 + (-5.09 \pm 0.11) \; \mu^2 \\ &+ (4.61 \pm 0.36) \; \mu^2 \; e^2] \end{split}$$

Here, a is the binary semimajor axis, e is the binary eccentricity, and $\mu = \mathcal{M}_1/(\mathcal{M}_1 + \mathcal{M}_2)$ is the mass ratio of the primary to the total mass.

5.2. Habitable Zone Calculation

HZ distances around stars are derived following the approach outlined by Kopparapu et al. (2013). The procedure begins by calculating the effective stellar flux, adjusted for

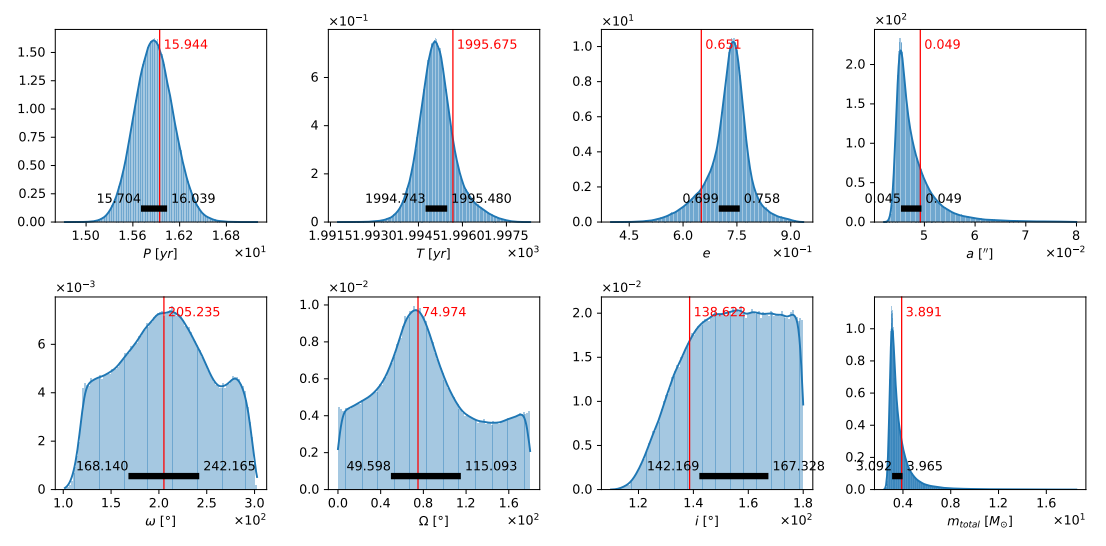


Figure 5. Parameter marginal posterior distributions.

Table 6Habitable Zone and Stellar Flux Table for HD 25811

Scenario	$S_{ m eff,Sun}$	а	b	С	d	$S_{ m eff,1}$	Primary HZ (au)	$S_{ m eff,2}$	Secondary HZ (au)
Recent Venus	1.7753	0.000143	2.9875e-09	-7.5702e-12	-1.1635e-15	1.948533	1.947459	1.938078	1.812943
Runaway Greenhouse	1.0512	0.000132	1.5418e-08	-7.9895e-12	-1.8328e-15	1.228919	2.452227	1.217133	2.287709
Moist Greenhouse	1.0140	0.000082	1.7063e-09	-4.3241e-12	-6.6462e-16	1.112952	2.576820	1.106980	2.398832
Maximum Greenhouse Early Mars	0.3438 0.3179	0.000059 0.000055	1.6558e-09 1.5313e-09	-3.0045e-12 -2.7786e-12	-5.2983e-16 -4.8997e-16	0.415970 0.384647	4.214940 4.383197	0.411544 0.380554	3.934245 4.091302

 Table 7

 Stability Distances and Habitable Zone Ranges for HD 25811 System

Parameter	Value (au)
S-type stability distance (nominal)	0.559
S-type stability distance (min)	0.341
S-type stability distance (max)	0.634
P-type stability distance (nominal)	38.220
P-type stability distance (min)	35.041
P-type stability distance (max)	38.451
HD 25811 A HZ range	1.947-4.383
HD 25811 B HZ range	1.813-4.091

stellar temperature differences compared to the Sun. The effective flux is calculated via:

$$S_{\text{eff}} = S_{\text{eff},\odot} + a \Delta T + b (\Delta T)^{2}$$

+ $c (\Delta T)^{3} + d (\Delta T)^{4},$ (15)

where $\Delta T = T_{\rm star} - T_{\odot}$, and a, b, c, and d are empirically determined coefficients.

The corresponding HZ distance is

$$d_{\rm HZ} = \sqrt{\frac{L/L_{\odot}}{S_{\rm eff}}}, \qquad (16)$$

where L/L_{\odot} is the star's luminosity relative to the Sun. Each star within the HD 25811 system has unique HZs determined individually. Table 6 summarizes the stellar flux and resulting HZ distances for different climate scenarios.

5.3. Habitable Zone Distances

Table 7 provides stability limits and HZ ranges for both circumstellar and circumbinary orbits in the HD 25811 system.

Figure 7 illustrates the overall habitability and stability regions for the complete HD 25811 binary system, while Figures 8 and 9 zoom in specifically on the regions around the primary and secondary stars, respectively. The shaded areas signify HZs, and dashed lines delineate stability boundaries where planetary orbits remain viable over long time periods.

This detailed analysis is crucial for evaluating the potential habitability of planets within binary star systems, highlighting

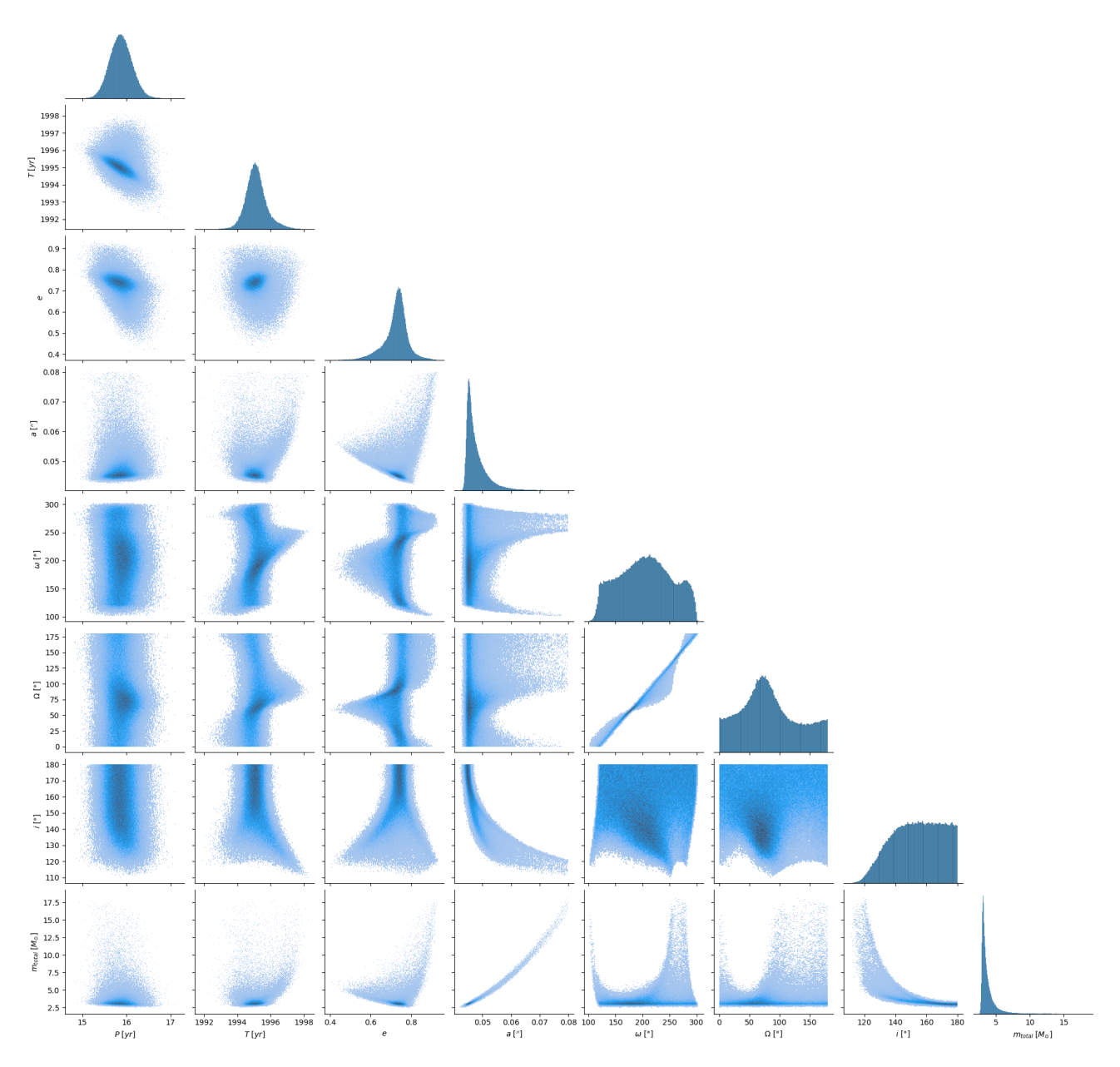


Figure 6. Parameter pair posterior distributions.

the strong influence of stellar properties on the extent and position of HZs.

6. Conclusion

This study utilized Al-Wardat's method to analyze the HD 25811 binary system, deriving precise stellar parameters for its individual components. The analysis revealed nearly identical effective temperatures of 7100 \pm 50 K for the primary component and 7000 \pm 50 K for the secondary component, with stellar masses of 1.65 \pm 0.15 M_{\odot} and 1.58 \pm 0.14 M_{\odot} , respectively. Both stars, which are estimated to be in the range

of 0.794 Gyr and 0.891 Gyr, and in their initial subgiant phase, supported by the synthetic evolutionary tracks and isochrones for $Z\!=\!0.03$, confirm their common origin and chemical homogeneity. The orbital analysis yielded a period of 15.97 yr, an eccentricity of 0.713, and a total system mass of $3.65\pm0.49\,M_{\odot}$. These results demonstrate the efficacy of Al-Wardat's method in determining accurate stellar parameters and underscore the system's value as a benchmark for studying binary star evolution.

A comprehensive analysis of the orbital stability and potential habitability regions within the HD 25811 binary star

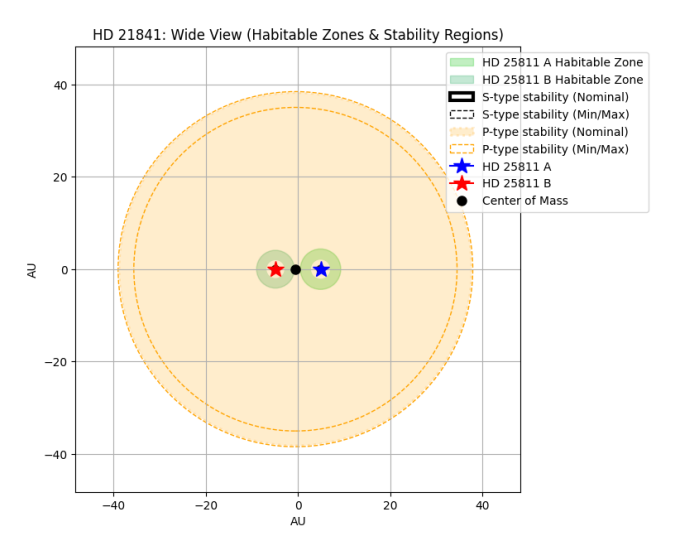


Figure 7. Habitability zones (green areas) and stability regions (dashed lines) for the HD 25811 entire binary system.

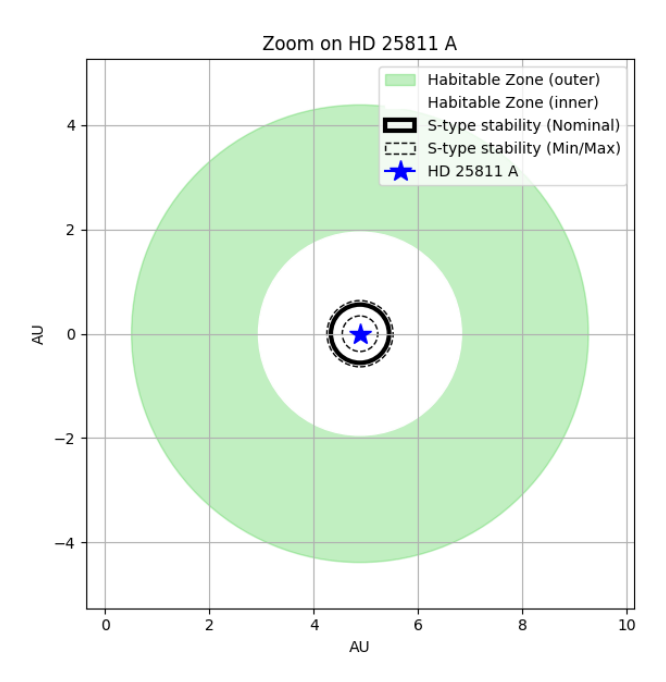


Figure 8. Habitability and stability zones around the primary star HD 25811 A.

system is presented in this study, which highlights critical stable zones for both circumstellar (S-type) and circumbinary (P-type) planets in the system, based on empirical stability criteria developed by Holman & Wiegert (1999). By calculating the boundaries of HZs according to Kopparapu et al. (2013), we have determined the extent of habitable regions influenced by stellar luminosity and temperature differences. Our results show that primary and secondary stars have distinct and precisely quantified stability ranges. It is evident

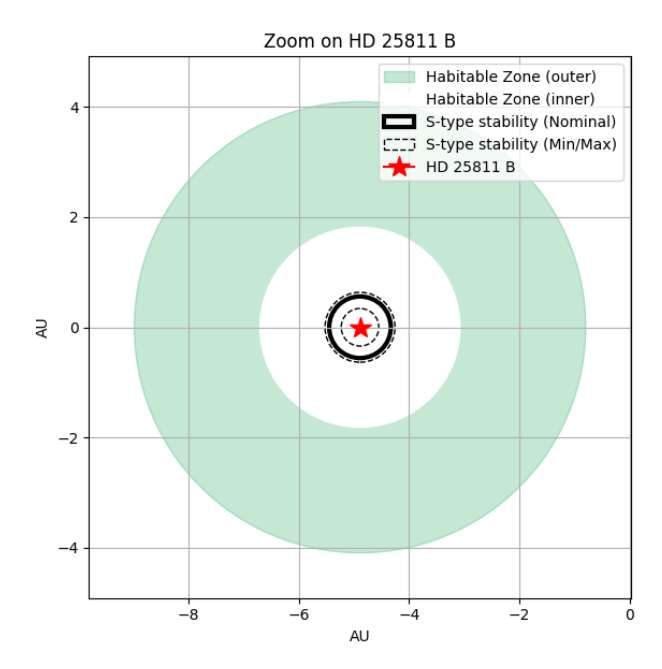


Figure 9. Habitability and stability zones around the secondary star HD 25811 B.

from these findings that stellar properties and planetary habitability are intertwined. Still, future observational and theoretical studies will also be able to identify exoplanets that could support life in binary stars.

Acknowledgments

This study utilized several resources and tools, including SAO/NASA, the SIMBAD database, the Fourth Catalog of Interferometric Measurements of Binary Stars, 2MASS, and IPAC data systems. It also utilized MCMC's orbital analysis code, and the codes of Al-Wardat's method for analyzing stellar systems.

ORCID iDs

Hassan B. Haboubi https://orcid.org/0009-0004-7254-0724 Mashhoor A. Al-Wardat https://orcid.org/0000-0002-1422-211X

Ahmad A. Abushattal https://orcid.org/0000-0002-7796-6562

References

Abushattal, A., Alrawashdeh, A., & Kraishan, A. 2022a, CoBAO, 69, 251 Abushattal, A., Al-Wardat, M., Taani, A., Khassawneh, A., & Al-Naimiy, H. 2019a, Journal of Physics: Conference Series, 1258, 012018

```
Abushattal, A., Kraishan, A., & Alshamaseen, O. 2022b, CoBAO, 69, 235
Abushattal, A. A., Al-Wardat, M. A., Horch, E. P., et al. 2024, AdSpR,
   73, 1170
Abushattal, A. A., Docobo, J. A., & Campo, P. P. 2019b, AJ, 159, 28
Al-Wardat, M., Docobo, J., Abushattal, A., & Campo, P. 2017, AstBu, 72, 24
Al-Wardat, M. A. 2002a, BSAO, 53, 51
Al-Wardat, M. A. 2002b, BSAO, 53, 58
Al-Wardat, M. A. 2003, BSAO, 56, 41
Al-Wardat, M. A. 2003, BSAO, 55, 18
Al-Wardat, M. A. 2007, AN, 328, 63
Al-Wardat, M. A. 2009, AN, 330, 385
Al-Wardat, M. A. 2012, PASA, 29, 523
Al-Wardat, M. A. 2014, AstBu, 69, 454
Al-Wardat, M. A., Abu-Alrob, E., Hussein, A. M., et al. 2021a, RAA, 21, 161
Al-Wardat, M. A., Balega, Y. Y., Leushin, V. V., et al. 2014a, AstBu, 69, 58
Al-Wardat, M. A., El-Mahameed, M. H., Yusuf, N. A., Khasawneh, A. M., &
   Masda, S. G. 2016, RAA, 16, 166
Al-Wardat, M. A., Hussein, A. M., Al-Naimiy, H. M., & Barstow, M. A.
   2021b, P
            ASA, 38, e002
Al-Wardat, M. A., Widyan, H. S., & Al-thyabat, A. 2014b, PASA, 31, e005
Alameryeen, H., Abushattal, A., & Kraishan, A. 2022, CoBAO, 69, 242
Algnamat, B., Abushattal, A., & Kraishan, A. 2022, CoBAO, 69, 223
Andersen, J. 1991, A&ARv, 3, 91
Balega, I., Balega, Y. Y., Maksimov, A. F., et al. 2004, A&A, 422, 627
Balega, I. I., & Balega, Y. Y. 1987, SvAL, 13, 208
Balega, I. I., Balega, Y. Y., Belkin, I. N., et al. 1994, A&AS, 105, 503
Balega, I. I., Balega, Y. Y., Hofmann, K.-H., & Weigelt, G. 2001, AstL, 27, 95
Balega, I. I., Balega, Y. Y., Hofmann, K.-H., et al. 2002, A&A, 385, 87
Balega, I. I., Balega, Y. Y., Hofmann, K.-H., et al. 2006, A&A, 448, 703
Balega, I. I., Balega, Y. Y., Maksimov, A. F., et al. 2007, AstBu, 62, 339
Balega, I. I., Balega, Y. Y., & Vasyuk, V. A. 1989, AISAO, 28, 107
Cannon, A. J., & Pickering, E. C. 1993, VizieR Online Data Catalog: Henry
   Draper Catalogue and Extension (Cannon+ 1918-1924; ADC 1989), yCat,
   III/135A Originally published in: Harv. Ann. 91-100 (1918-1924)
Claveria, R. M., Mendez, R. A., Silva, J. F., & Orchard, M. E. 2019, PASP,
   131, 084502
Cockell, C. S., Bush, T., Bryce, C., et al. 2016, AsBio, 16, 89
Cutri, R. M., Skrutskie, M. F., van Dyk, S., et al. 2003, VizieR Online Data
   Catalog: 2MASS All-Sky Catalog of Point Sources (Cutri+ 2003), yCat,
   II/246 2MASS Point Source Catalogue, sample output; (on a total of
   470,992,970 sources)
Docobo, J., Balega, Y., Campo, P., & Abushattal, A. 2018, Double Stars Inf.
   Circ., 196, 1
Docobo, J. A., Griffin, R. F., Campo, P. P., & Abushattal, A. A. 2017,
      IRAS, 469, 1096
ESA 1997, yCat, I/239
```

Evans, D. S., Edwards, D. A., Frueh, M., McWilliam, A., & Sandmann, W. H.

1985, AJ, 90, 2360

Gaia Collaboration 2018, yCat, I/345

Gaia Collaboration 2020, yCat, I/350

```
Gaia Collaboration 2022, yCat, I/355
Gaia Collaboration, Brown, A. G. A., Vallenari, A., et al. 2016, A&A, 595, A2
Girardi, L., Bressan, A., Bertelli, G., & Chiosi, C. 2000a, A&AS, 141, 371
Girardi, L., Bressan, A., Bertelli, G., & Chiosi, C. 2000b, yCat, J/A+AS/
  141/371, Originally published
Gray, D. F. 2021, The Observation and Analysis of Stellar Photospheres (4th
  ed.; Cambridge: Cambridge Univ. Press)
Hartkopf, W. I., McAlister, H. A., & Franz, O. G. 1992, AJ, 104, 810
Høg, E., Fabricius, C., Makarov, V. V., et al. 2000, A&A, 355, L27
Holman, M. J., & Wiegert, P. A. 1999, AJ, 117, 621
Hussein, A. M., Al-Wardat, M. A., Abushattal, A., et al. 2022, AJ, 163, 182
Kopparapu, R. K., Ramirez, R., Kasting, J. F., et al. 2013, ApJ, 770, 82
Lang, K. R. 1992, Astrophysical Data I. Planets and Stars (Verlag Berlin
  Heidelberg New York: Springer), 937
Masda, S., & Al-Wardat, M. 2023, AdSpR, 72, 649
Masda, S., Al-Wardat, M., Aljboor, H., et al. 2025, RAA, 25, 025011
Masda, S., Yousef, Z. T., Al-Wardat, M., & Al-Khasawneh, A. 2023, RAA,
  23, 115005
Masda, S. G., Al-Wardat, M. A., & Moula Khan Pathan, J. K. 2018, RAA,
  18, 072
Masda, S. G., Al-Wardat, M. A., Neuhäuser, R., & Al-Naimiy, H. M. 2016,
  RAA, 16, 112
Masda, S. G., Khan, A. R., & Pathan, J. M. 2021, Photometric solution of
   visual binary system: HIP57894, in 4th Int. Conf. on Emerging
   Technologies; Micro to Nano, 2019 (ETMN 2019), 2335 (Pune, India,
  16-17 December 2019) (Melville, NY: AIP), 090002
Mason, B. D., Tokovinin, A., Mendez, R. A., & Costa, E. 2023, yCat, J/AJ/
   166/139, Originally published
McAlister, H., Hartkopf, W. I., & Franz, O. G. 1990, AJ, 99, 965
McAlister, H. A., Hartkopf, W. I., Hutter, D. J., & Franz, O. G. 1987, AJ,
  93, 688
McAlister, H. A., Hartkopf, W. I., Sowell, J. R., Dombrowski, E. G., &
  Franz, O. G. 1989, AJ, 97, 510
Mendez, R. A., Claveria, R. M., Orchard, M. E., & Silva, J. F. 2017, AJ,
   154, 187
Schlafly, E. F., & Finkbeiner, D. P. 2011, ApJ, 737, 103
Schmidtke, P. C., & Africano, J. L. 1984, AJ, 89, 1371
Sterken, C. 2007, in ASP Conf. Ser. 364, The Future of Photometric,
  Spectrophotometric and Polarimetric Standardization (San Francisco,
  CA: ASP),
Szebehely, V. 1984, CeMec, 34, 49
Tokovinin, A., Mason, B. D., Hartkopf, W. I., Mendez, R. A., & Horch, E. P.
  2016, AJ, 151, 153
Tokovinin, A., Mason, B. D., Mendez, R. A., & Costa, E. 2022, AJ, 164, 58
Tokovinin, A., Mason, B. D., Mendez, R. A., & Costa, E. 2024, AJ, 168, 28
Tokovinin, A., Mason, B. D., Mendez, R. A., Costa, E., & Horch, E. P. 2020,
  yCat, J/AJ/160/7
Tokovinin, A., Mason, B. D., Mendez, R. A., Horch, E. P., & Briceño, C.
   2019, AJ, 158, 48
Tokovinin, A., Mason, B. D., Mendez, R. A., et al. 2021, AJ, 162, 41
```